Self detachment of free-standing porous silicon membranes in moderately doped n-type silicon

**Neeraj Kumar · Salvatore Gennaro ·
Pradeep Vallachira Warriam Sasikumar ·
Gian Domenico Sorarù · Paolo Bettotti**

Abstract In this article we describe a reliable etching method to fabricate porous silicon free-standing membranes (FSMs) based on a self detachment of the porous layer in moderately doped n-type silicon substrates. We found that stable growth of smooth and straight pores is restricted to a narrow range of etching conditions and, unlike p-type substrates, the lift-off of the membrane is a self-limited process that does not require a large burst of current. The detachment of the porous membrane is independent of the structure of the already porosified layer, meaning that the average pore diameter can be tuned from nano to macro size within the same membrane. We also demonstrate that, despite their limited thickness, FSMs are quite robust and can sustained further processing. Thus, the etching receipt we are proposing here extends the range of sensors and filters that can be fabricated using porous silicon technology.

1 Introduction

Good control over the structure of porous materials is a formidable task and it is of fundamental importance to tailor and control their properties. Over the last few decades porous silicon (PSi) has attracted a remarkable level of interest due to the high degree of flexibility given by electrochemical etching to tune its optical, electrical and mechanical properties. PSi is still actively investigated for the development of sensors [1], filters [2], drug-release materials [3, 4], photovoltaic (PV) [5] and thermoelectric [6–8] systems and it finds applications in microelectronics (e.g. as in Bosch APSM© technology).

Despite its long history, the control over PSi porous structure is still a matter of research, particularly for pore sizes between a few tens and a few hundred nanometers. This submicron regime can be obtained in substrates with resistivity in the range of 0.01–1 Ω cm and it is of interest for the fabrication of filters and sensors, because the pores have a length scale comparable to that of biological relevant structures and they are also compatible with fluidics applications. Several articles were published about the fabrication of free-standing membranes (FSMs) in p-type silicon [9–11], but the limited anisotropy of the etching in this substrate produces two main limits: (1) the pores always have a conical shape with the top part of the pores significantly larger than the bottom part; (2) such high-porosity superficial layers are often damaged due to the surface tension of the liquid, which makes the pore walls collapse [12].

N-type silicon is less investigated because light-assisted etching is not effective at these doping levels and the porosification is performed on a reversed biased electrochemical junction [13–15]. This means that small variations in either doping concentration or current density translate into a large variation of the porous structure [16]. Only recently the fabrication of small fragments of free-standing double microporous layers on heavily doped n-type (0.001–0.003 Ω cm) silicon have been reported for the first time [17] but, till now, no evidence about the

N. Kumar · P. Bettotti (✉)
Nanoscience Laboratory, Department of Physics, University of Trento, Via Sommarive 14, 38123 Povo, TN, Italy
e-mail: paolo.bettotti@unitn.it
URL: http://www.science.unitn.it/~semicon/

S. Gennaro
MinaLab, FBK, via Sommarive 16, 38123 Povo, TN, Italy

P. V. W. Sasikumar · G. D. Sorarù
Department of Materials Engineering and Industrial Technology, University of Trento, 38050 Trento, Italy

possibility to detach thin membranes of macroscopic size was reported on n-type silicon.

Despite these difficulties, moderately doped n-type Silicon (0.01–0.1 Ω cm) is an ideal candidate for the fabrication of porous membranes with well controlled and tailored properties and it overcomes most of the limits found in the p-type material. They permit the fabrication of submicron pores (30–100 nm) opened at both ends, with constant cross section and with no pore size shrinking on the superficial layer [18]. Such structure is of great interest to develop biosensors because it satisfies two key parameters: it is compatible with mass transport through the porous membrane (and this fact maximizes the binding efficiency and reduces the assay time). Moreover, pore size is still much smaller than visible wavelengths; thus, the optical quality of the structure is not severely reduced compared to truly nanoporous sponges typically obtained in highly doped substrates [19].

Recently, the possibility to obtain high aspect ratio (and fast growth) of pores in n-type substrate exploiting the reverse bias mechanism has been demonstrated [20]. Similar structures were never reported for p-type silicon, because of the reduced anisotropy of the etching in this substrate (such limited anisotropy is particularly evidenced in macroporous structures such as in [21]). In this article, we report for the first time a robust fabrication method to produce large area FSMs with pore size tunable across the submicron range etched in moderately doped n-type silicon. We found that membrane detachment is a self-limited process that involves the formation of a thin transitional layer at the bottom of the porous region and, thus, no high burst of current have to be applied to detach them. On the other hand, given a certain doping level, this fact poses a limit to the maximum membrane thickness achievable. This is a striking difference that characterizes moderately doped n-type substrates from both lightly and heavily doped p- and n-type wafers.

The etching receipt we propose here permits the pore size to be tuned over a broad range of dimension and maintains a very good planarity among the layers interfaces. Thus, multilayer samples with high optical quality and mechanically robust FSMs can be obtained. As an example, to show the mechanical strength of the thin membranes, they are subjected to a layer transfer process (LTP). The LTP is referred to with a variety of names in the literature (silicon-on-nothing [22], Advanced Silicon Microfabrication Technique, chipfilm [23] and is a method to fabricate thin- and quasi-crystalline layers starting from a porous bilayer and exploiting atomic diffusion driven by a thermal annealing in an inert atmosphere. Both AFM surface morphology and Raman analysis confirm the high quality of the re-crystallized PSi after the annealing process in an argon atmosphere.

Despite the fact that this article is not focused on the fabrication of large-area thin layer of crystalline silicon for photovoltaic applications using the LTP process, the substrates investigated here may be used to develop low-cost n-type Silicon-based photovoltaic cells [24].

2 Experimental

Samples were fabricated using n-type silicon wafer (0.01–0.02 Ω cm), polished on one side and oriented along the [100] crystalline direction. The anodizing was performed at room temperature in the absence of light and a computer-controlled current source was used to control the applied current density. Etching solutions were composed of aqueous HF 12 % (starting from aqueous HF 48 %) and 20 % H_2O_2. While the HF and H_2O_2 concentrations were kept fixed, we tested two different solvents to investigate the role of the oxidant species: in one case we use a solution of 1:1 volumetric ratio of water and ethanol (hereafter called aqueous solution); in the other case we added only ethanol to the concentrated HF solution (hereafter called ethanoic solution). After fabrication of the porous layers, all samples were rinsed in ethanol and dried in a N_2 flow. The structural morphology of the PSi sample was investigated using scanning electron microscopy (SEM, JEOL mod. JSM 7401F). The surface morphology and roughness of annealed double-porosity layer (DPL) samples were investigated using atomic force microscopy (AFM, NTMDT mod. P47H) working in contact mode. Raman measurements (Labram Aramis from JobinYvon Horiba) were also performed to check the crystallinity of the annealed PSi layers.

3 Results and discussions

3.1 Optimization of the porous structure

For a given silicon resistivity, the HF concentration and applied current density are the two key parameters that determine the PSi structure (i.e. micro < 20 nm, meso < 50 nm and macro > 50 nm) [25]. Results obtained on similar substrates by previous studies suggest that pore size increases with decreasing HF concentration [18].

It is known that porosity is inversely proportional to HF concentration, thus initially we used 6 % HF solutions. This HF concentration shows an etch rate of only 3 nm/s while applying the largest current density (14 mA/cm^2), which allows the etching of samples several microns thick, without electro-polishing them. Moreover, the etched pores are highly branched. We found that using 12 % HF it was possible to obtain larger and smooth pores while retaining the ability to detach membranes.
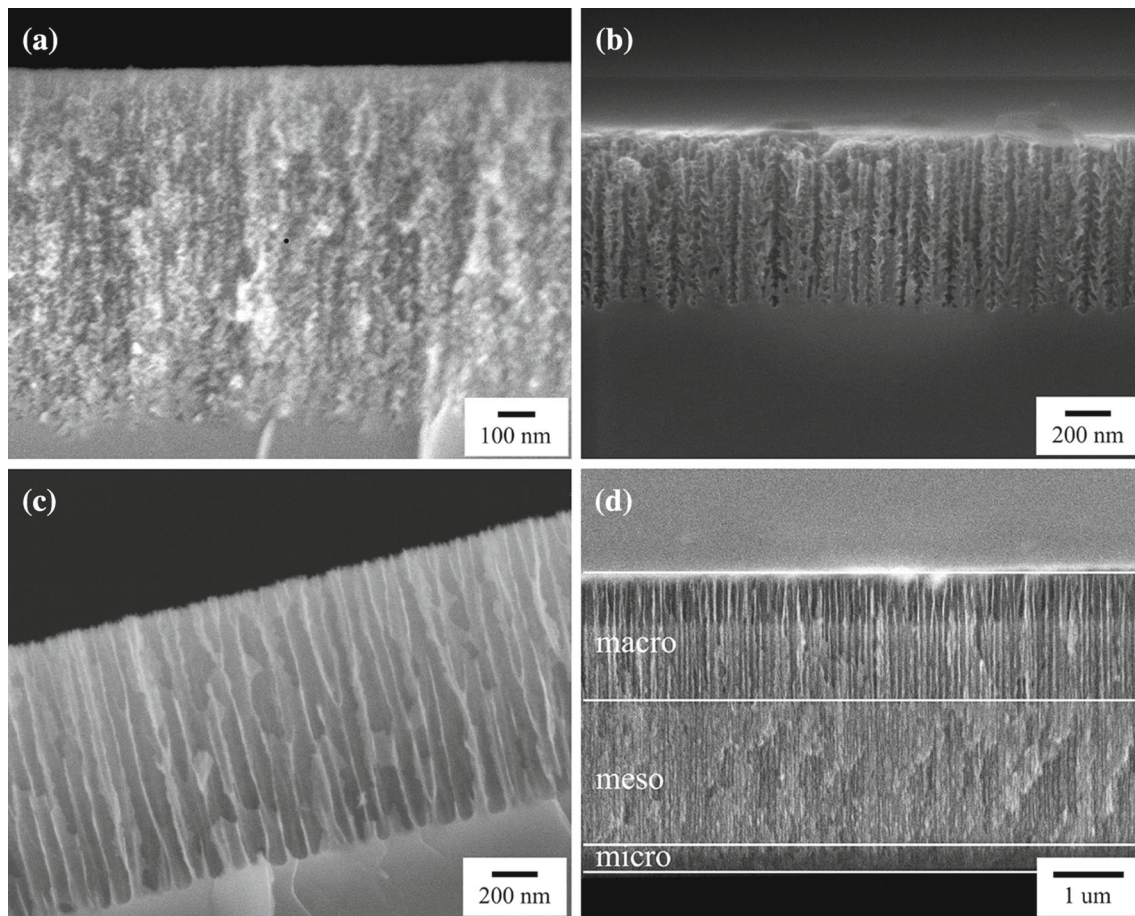
Fig. 1 a–c show cross-sectional SEM images of n-type PSi etched using ethanoic solution. Current densities are, respectively, 4, 20 and 80 mA/cm^2. Similar structures are obtained using aqueous solutions.

d Cross section of a multilayer composed of macroporous (*top*), mesoporous (*center*) and microporous (*bottom*) layers

Figure 1a–c summarizes the limiting structures that can be obtained using ethanoic solutions at low and large current densities, respectively. As expected, both pore size and etch rate increase with current density. Rough, tree-like (micro–meso) porous structures develop at low current density using both types of solutions, while smooth and straight macropores grow when the current increases. Very similar structures are also obtained using the aqueous-based solution. The two main differences induced by the use of water-based solutions are (1) a larger current density is required to obtain smooth pores and (2) both pore size and etch rates slightly increase. Careful optimization of the etching solution allowed us to obtain homogeneous PSi layers and to fabricate large area, free-standing multilayers with micro–meso and macropores within the same membrane. Figure 1d shows a multilayer cross section. Starting from the top surface: two macroporous layers are shown etched at 60 and 80 mA/cm^2, a middle mesoporous layer was etched using 40 mA/cm^2 and a bottom microporous layer was fabricated applying 4 mA/cm^2. Flat interfaces between each layer are clearly visible from the SEM image.

Figure 2a, b summarizes these key features versus the applied current density for ethanoic and aqueous solutions, respectively. Etch rates range from 15 to 30 nm/s, at 20 and 80 mA/cm^2, respectively, and are similar for both solvents. When using the ethanoic-based solution the resulting pores have a pore diameter of around 30 nm at 20 mA/cm^2, which increases to around 80 nm using a current density of 60 mA/cm^2. On the other hand using an aqueous solution, pores are slightly larger (up to 100 nm). The threshold to obtain straight and smooth pores depends on the solution composition: it is smaller using ethanoic solution (60 mA/cm^2) and it increases with aqueous solution (80 mA/cm^2). This is probably due to the higher polishing current density that is sustained by solutions containing oxidants. It is notable that pores are perfectly open up to the surface of the PSi.

3.2 Fabrication of free-standing double-porosity layers

Compared to p-type Si the most striking difference concerns the detachment of the membrane. In highly to moderate doped n-type substrates, while the top layer thickness

(a)

(b)
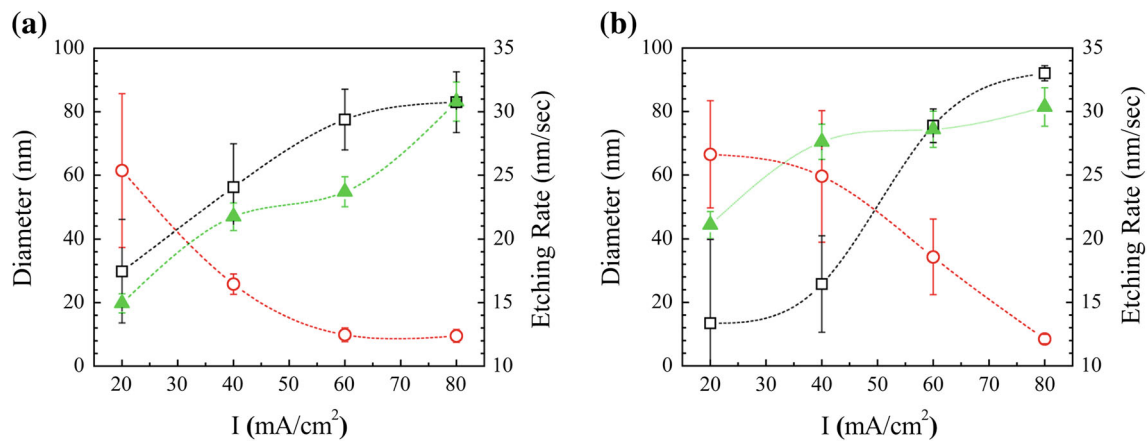
Fig. 2 Key structural parameters and etch rate of PSi samples. Pore diameter (*left axis, black open squares*), pore wall thickness (*left axis, red open circles*) and etch rate (*right axis, green filled triangles*).

a Data for samples etched in ethanol-based solution, **b** data for aqueous solution. *Dotted lines* are included to guide the eye

can be chosen at will by varying the etching time, the thickness of the transitional layer is nearly fixed. Once the solution composition has been fixed, the time (t_L) at which membrane lifts-off from the substrate (and thus the thickness of this bottom layer) can only be slightly tuned by modifying the applied current density, as shown in Fig. 3a. For a current density of 60 mA/cm^2, t_L approaches ∼75 s (225 s) corresponding to a thickness of around 1.5 µm (5.5 µm) for ethanoic (aqueous) solution and decreases down to roughly 35 s (70 s) for 80 mA/cm^2 corresponding to 900 nm (2.1 µm) thick transitional layer.

The origin of the self detachment of the FSMs is still not completely clear. To our best knowledge this behavior is only reported for moderate and highly doped n-type substrate. It is known that diffusion-limited transport along the pores produces a gradient of the HF concentration. The net result is to introduce instability in the pore growth and pore diameter tends to increase with the pore depth. When the wall between two neighbor pores is completely etched, the membrane detach from the substrate [12]. The etching conditions we are reporting constitute a significant improvement: the pore size can be tuned over a broad range of dimensions and the detachment is independent from the pore size of the last etched layer (as shown in Fig. 1d). Such differences are reasonably due to the balance among the wafer doping levels we are considering and the addiction of oxidants to the etching solution. Oxidants increase the average pore diameter and reduce the waviness of the pore surface. Thus, they facilitate the fabrication of high-porosity layer that is easily brought into the electropolishing regime and permit to form a sharp detachment interface independently from the structure of the previously formed PSi layer. In addition, Fig. 3b shows one of the FSM DPLs fabricated: the sample is 2 µm thick and 13 mm in diameter and it was transferred on a glass substrate.

To optimize LTP the top PSi layer should have small and homogeneous pores such that, after annealing, a nearly flat, re-crystallized surface can be obtained. In our study we use a current density of 20 mA/cm^2 for the low-porosity layer and 80 mA/cm^2 for the high porosity (for both solutions considered). Figure 3c shows a SEM cross section of a DPL just before its release. The two porous layers are clearly visible, as well as the nearly completely etched interface where DPL detaches from the underlying bulk silicon. Figure 3d reports the iV curve corresponding to the fabrication of a DPL: the first plateau at constant voltage corresponds to the formation of the upper, low-porosity layer. The second step forms the lower, high-porosity layer. As for p-type Si, a sudden increase in the voltage indicates the membrane detachment from the underlying substrate [17, 26].

3.3 Surface characterization and crystallinity of the DPL

PSi for LTP applications should have a minimum of stress and structural disorder. In this way the mechanical strength of the membrane is increased and they can sustain further processing [27, 28]. We fabricate several DPLs on a silicon substrate with the above-mentioned solutions. Their structure is similar to that reported in Fig. 3c and are composed by a 2 µm thick low-porosity top layer (with roughly 10 nm pore size) and a 300 nm thick high-porosity bottom layer (with nearly 90 nm pore size). To remove the stress and re-crystallize the material, all DPLs were annealed at 1,100 °C for different times (30, 60 and 120 min) in an argon atmosphere. AFM images on DPL samples annealed for 0 and 120 min are shown in Fig. 4a, b, respectively. AFM analysis reveals that surface roughness decreases significantly with increasing annealing time. Before etching, the mono-crystalline Si wafer used has
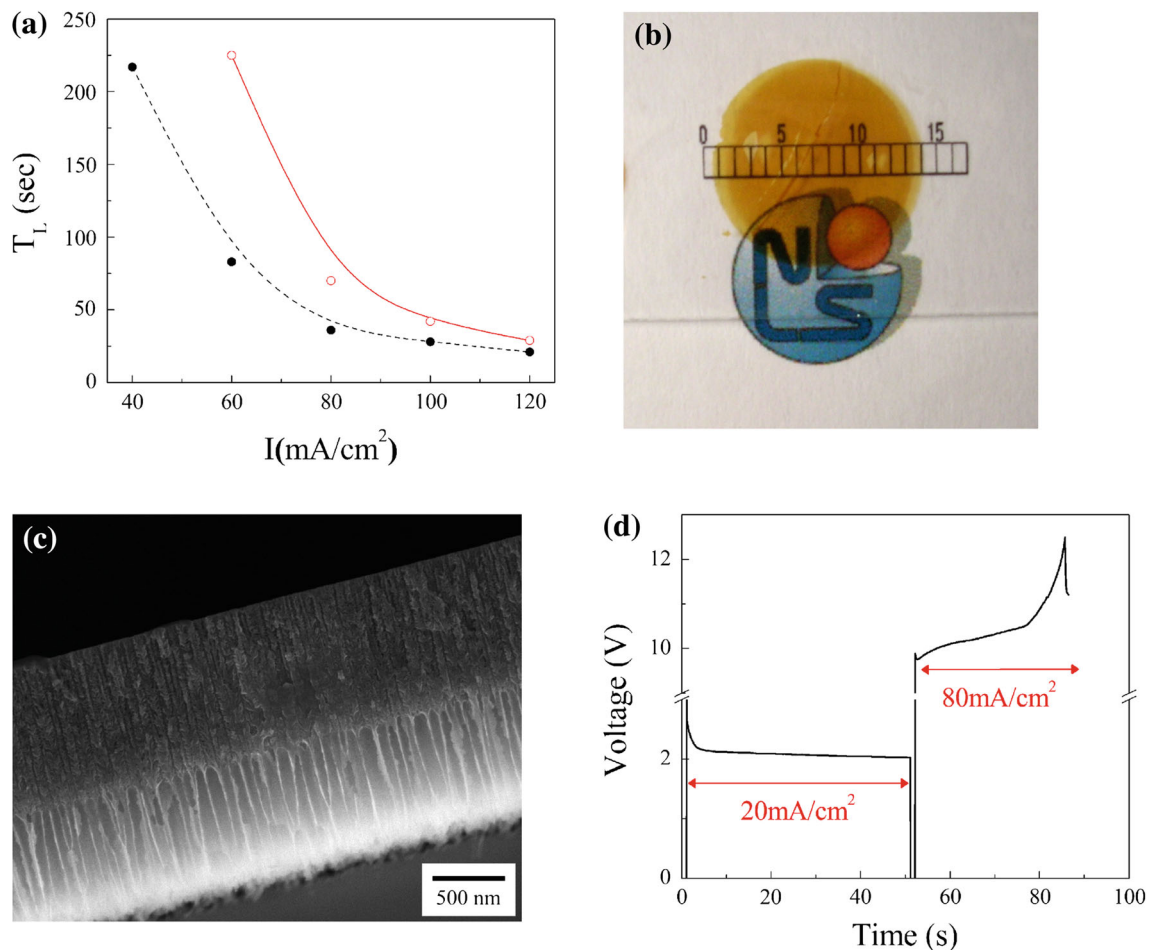
Fig. 3 **a** Relation between applied current density and lift-off time for the porous layer in aqueous (*red open symbols*, *solid line*) and ethanoic (*black filled symbols*, *dotted line*) solution. **b** Photograph of a complete detached n-type PSi free-standing double layer (~ 2 μm) released on a glass substrate. The small cracks visible are created during the sample handling and are not due to sample inhomogeneity.

Scale bar unit mm. **c** SEM cross section of a DPL just before detachment. The two porous layers and the detachment interface are clearly visible. **d** iV curve corresponding to the fabrication of a DPL membrane. Current densities used to fabricate each layer are shown in *red*

average root mean square (rms) surface roughness of around 0.2 nm. Figure 4c reports the trends of rms versus annealing time. Non-annealed sample have an rms of 2.4 nm for aqueous and 4.8 nm for ethanoic solutions. After 2 h annealing, the rms surface roughness reduces to 0.5 nm for aqueous solution and 0.7 nm for samples etched in ethanoic solution. It is of interest to note that, despite the larger initial pore sizes in the top layer, samples etched using mixed solutions systematically present smaller rms roughness values compared to samples etched in ethanol based solutions.

The quality of re-crystallization induced by the annealing was further investigated by Raman spectroscopy. The Si substrate shows the usual Raman peak at $520/cm^{-1}$ having FWHM $\sim 3.5/cm^{-1}$ (calculated by fitting the peak with a Lorentzian function), shown in Fig. 4d. In DPL samples, the Raman peak shifts slightly towards higher energy and a shoulder appears to its low-energy side. This

deformation is compatible with a stressed Si lattice [29], due to the nanoporous structure, but there is no clear evidence of the amorphous silicon phase (a broad band at $480/cm^{-1}$). With increasing annealing time the peak contracts and recovers its original position at lower energy. A 2 h long anneal is sufficient to recover a crystalline structure comparable with the initial one (FWHM $\sim 3.8/cm^{-1}$).

4 Conclusions

In this article, we demonstrate that a careful optimization of the anodizing process in HF acid allows the production of large area, porous silicon, FSMs on moderately doped n-type silicon substrate (0.01–0.02 Ω cm). The average pore size can be tuned from less than 20 nm up to 100 nm and macroscopic FSMs only few microns thick can be routinely fabricated and transferred to different substrates
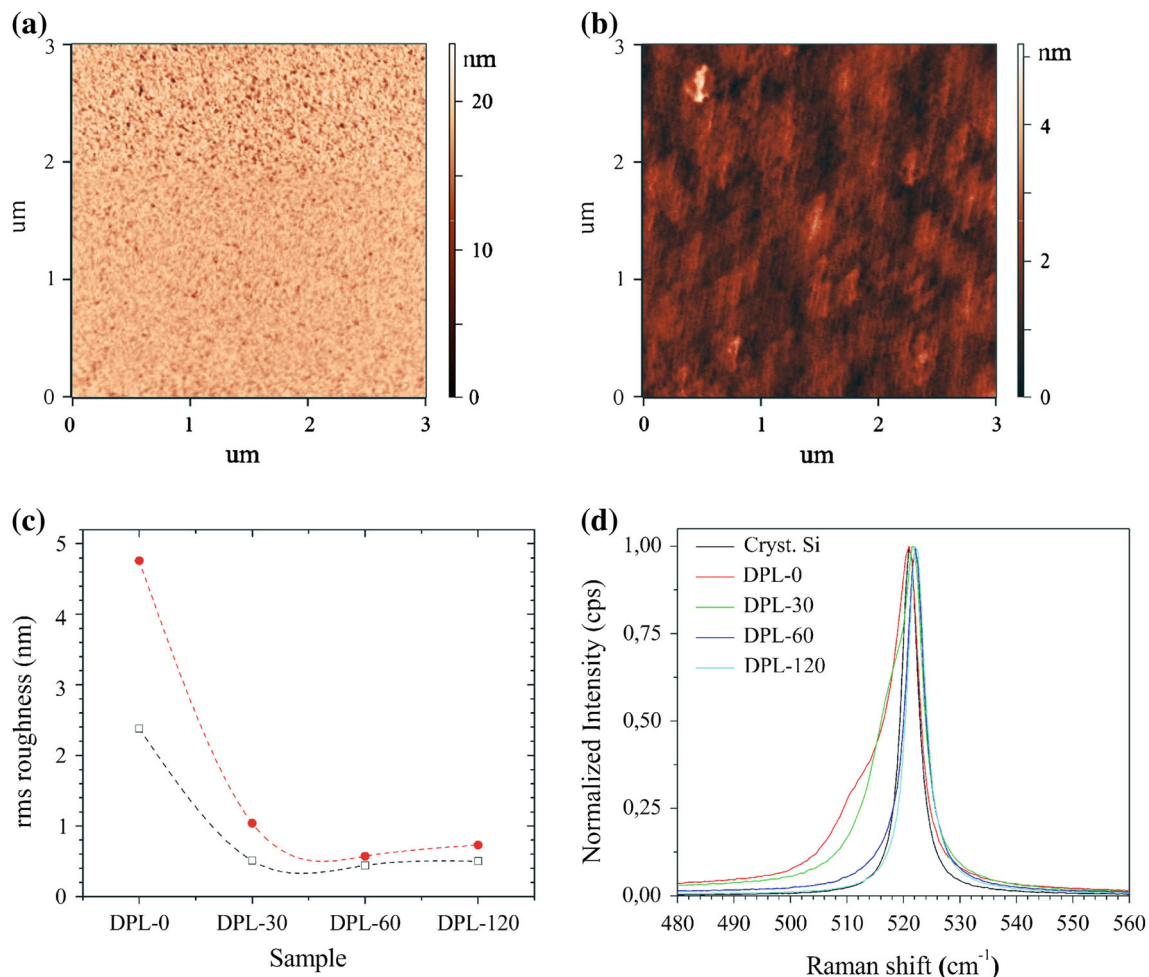
Fig. 4 a, **b** AFM images on DPL samples annealed for 0 and 120 min respectively. **c** RMS surface roughness obtained from AFM images of DPL samples annealed for different lengths of time (0, 30, 60 and 120 min). *Empty symbol* refer to aqueous solution, while *filled* *circles* are for ethanoic solution. **d** Raman peak evolution for crystalline and annealed samples prepared with mixed solution. The different annealing times (in min) are indicated in the *legend within the figure*

(the aspect ratio of the membrane is around 7,000). No HF gradient effect was noted during the porous silicon etching and straight (not interconnected) macropores with a constant cross section develop. A notable difference compared to p-type substrates is that the membrane lift-off does not require any high burst current, but is a self-limited process, mainly dictated by the solution composition. We demonstrate that medium doped n-type silicon is also fully compatible with the fabrication of multilayer structures and that FSMs are mechanically robust and can sustain further processing (i.e. by LTP).

Our approach greatly increases the possibilities for fabricating thin FSMs of well-controlled morphology on n-type silicon. The length scale of the porous structures investigated here is of interest in many application fields: from biosensor to filtering devices, self cleaning surfaces based on hierarchical structures and low-cost photovoltaic systems based on thin film technologies.

References

1. J. Alvarez, P. Bettotti, I. Suarez, N. Kumar, D. Hill, V. Chirvony, L. Pavesi, J. Martinez-Pastor, Opt. Express **19**, 26106 (2011)
2. L.M. Bonanno, L.A. DeLouise, Biosens. Bioelectron. **23**, 444 (2007)
3. E.C. Wu, J.S. Andrews, L.Y. Chen, W.R. Freeman, L. Pearson, M.J. Sailor, Biomaterials **32**, 1957 (2011)
4. E. Gultepe, D. Nagesha, S. Sridhar, M. Amiji, Adv. Drug. Deliver. Rev. **62**, 305 (2010)
5. A. Wolf, B. Terheiden, R. Brendel, Prog. Photovoltaics **15**, 199 (2007)
6. G. Yuan, R. Mitdank, A. Mogilatenko, S.F. Fischer, J. Phys. Chem. C **116**, 13767 (2012)

7. J. de Boor, D.S. Kim, X. Ao, D. Hagen, A. Cojocaru, H. Foll, V. Schmidt, EPL **96**, 16001 (2011)

8. J. Tang, H.-T. Wang, D.H. Lee, M. Fardy, Z. Huo, T.P. Russell, P. Yang, Nano Lett. **10**, 4279 (2010)

9. J.H. Peterman, D. Zielke, J. Schmidt, F. Haase, E.G. Rojas, R. Brendel, Prog. Phtovol. Res. Appl. **20**, 1 (2012)

10. M. Ghulinyan, C.J. Oton, G. Bonetti, Z. Gaburro, L. Pavesi, J. Appl. Phys. **93**, 9274 (2003)

11. H. Koyama, F.M. Fauchet, J. Appl. Phys. **87**, 1788 (2000)

12. V. Lehmann, R. Stengl, A. Luigart, Mater. Sci. Eng. B **69**(70), 11–22 (2000)

13. H. Ouyang, M. Christophersen, P.M. Fauchet, Phys. Stat. sol. (a) **202**, 1396 (2005)

14. P. Granitzer, K. Rumpf, P. Polt, A. Reichmann, H. Krenn, Phys. E **38**, 205 (2007)

15. F.A. Harraz, S.M. El-Sheikh, T. Sakka, Y.H. Ogata, Electrochim. Acta **53**, 6444 (2008)

16. V. Lehmann, R. Stengl, A. Luigart, Mat. Sci. Eng **B69**, 11 (2000)

17. Y. Xiao, X. Li, H.-D. Um, X. Gao, Z. Guo, J.-H. Lee, Electrochim. Acta **74**, 93 (2012)

18. X.G. Zhang, *Electrochemistry of silicon and its oxide* (Kluwer Academic Publisher, New York, 2001)

19. J. Alvarez, C. Serrano, D. Hill, J. Martinez-Pastor, Opt. Lett. **38**, 1058 (2013)

20. D.H. Ge, J.W. Jiao, S. Zhang, Y.L. Wang, Electrochem. Commun. **12**, 603 (2010)

21. P. Bettotti, L. Dal Negro, Z. Gaburro, L. Pavesi, A. Lui, M. Galli, M. Patrini, F. Marabelli, J. Appl. Phys. **92**, 6966 (2002)

22. T. Yonehara, K. Sakaguchi, N. Sato, Appl. Phys. Lett. **64**, 2108 (1994)

23. J.N. Burghartz, W. Appel, H.D. Rempp, M. Zimmermann, IEEE Trans. Electron Devices **56**, 321 (2009)

24. R.C.G. Naber, N. Guillevin, A.R. Burgers, L.J. Geerligs, A.W. Weeber, *IEEE Photovoltaic Specialists Conference*, 5411189, 000990 (2009)

25. C.S. Solanki, R.R. Bilyalov, J. Poortmans, J.-P. Celis, J. Nijs, R. Mertens, J. Electrochem. Soc. **151**, C307 (2004)

26. P.C. Searson, Appl. Phys. Lett. **59**, 832 (1991)

27. M.B. Joshi, S.L. Hayashi, M.S. Goorsky, Electrochem. Solid State Lett. **11**, H236 (2008)

28. J. Van Hoeymissen, V. Depauw, I. Kuzma-Filipek, K. Van Nieuwenhuysen, M. Recaman Payo, Y. Qiu, I. Gordon, J. Poortmans, Phys. Stat. Sol. (a) **208**, 1433 (2011)

29. S. Manotasa, F. Agullo-Ruedaa, J.D. Morenob, F. Ben-Handerb, J.M. Martinez-Duart, Thin Solid Films **401**, 306 (2001)